Lighting Enhancement and Skin Lesion Analysis in Macroscopic Images using Genetic Algorithms and Deep Neural Networks

Vanesa Gómez-Martínez[1] and Cristina Soguero-Ruiz*[1]

[1]Department of Signal Theory and Communications, Rey Juan Carlos University, Madrid, 28943, Spain
{vanesa.gomez, cristina.soguero}@urjc.es

1 Introduction

Skin cancer is one of the most common cancers globally, with early detection crucial for better outcomes [1]. While dermoscopy is the gold standard [2], macroscopic imaging via smartphones offers a more accessible, low-cost alternative [3], though often affected by poor contrast, lighting, and sharpness—hindering automated diagnosis.

Existing methods like Intensity Equalization and Contrast Enhancement Techniques (IECET) [3] rely on paired images and focus mainly on brightness. We propose an unsupervised enhancement pipeline using genetic algorithms (GAs) [4] to optimize brightness, contrast, and sharpness without reference data. Enhanced images are processed via U-Net variants [5] for segmentation and ResNet-50 [6] for melanoma classification. We also apply Grad-CAM [7] for interpretability and bias analysis.

2 Materials and Methods

2.1 Dataset

We used a public dataset from the University of Waterloo [8, 9], containing 206 macroscopic skin lesion images (119 melanomas, 87 not melanomas) with expert-annotated segmentation masks.

2.2 Genetic algorithms for macroscopic image enhancement

GAs are unsupervised optimization methods inspired by natural selection [4]. In our approach, each chromosome encodes brightness, contrast, and sharpness parameters. A population of 50 chromosomes evolves over 40 generations, guided by our proposed fitness function Q, which combines three image quality metrics reflecting key aspects of medical image quality—enhancing lesion texture, borders, and tonal variation [10].

- **Contrast** (C): measures intensity variation between pixels and their neighbors, defined as: $C = \frac{1}{N_{\text{levels}}} \sum_{i=1}^{N_{\text{levels}}} \sum_{j=1}^{N_{\text{levels}}} (i-j)^2 \cdot P(i,j)$, where $P(i,j)$ is the gray-level co-occurrence matrix.
- **Brightness** (B): average intensity of the pixels in the image: $B = \frac{1}{N_{\text{pixels}}} \sum_{i=1}^{M} \sum_{j=1}^{N} I(i,j)$, where $I(i,j)$ is the grayscale value of pixel (i,j).
- **Sharpness** (Ni): computed as the variance of the Laplacian: $Ni = \text{Var}(\text{Laplacian}(I))$.

The final quality score is computed as a normalized weighted sum: $Q = \frac{C_{\text{enh}}}{C_{\text{orig}}} + \frac{B_{\text{enh}}}{B_{\text{orig}}} + \frac{Ni_{\text{enh}}}{Ni_{\text{orig}}}$. Chromosomes with higher Q values are favored during evolution, leading to optimal enhancement parameters.

2.3 U-Net and CNNs for skin lesion segmentation and classification

For skin lesion segmentation, we used the U-Net architecture and two variants: Attention U-Net (Att-Net) and Dense U-Net (D-Net) [5], which leverage an encoder-decoder structure to capture spatial and contextual features. Models were trained with Dice loss [11]. For melanoma classification, we employed ResNet-50 [6], a robust CNN for image tasks, trained with binary cross-entropy loss [12].

3 Results

3.1 Experimental setup

We conducted 5-fold cross-validation on the Waterloo dataset, using 80% of the data for training (15% for validation) and 20% for testing. Details of the experimental settings are summarized in Table 1.

Table 1. Summary of experimental setup.

Component	Configuration
Training parameters	
GA	P=50, G=40, $C\in[0.8, 1.2]$, $B\in[-10, 10]$, M=20%
U-Net	Opt: Adam, BS: 16, ES: 55 epochs, loss: Dice
ResNet-50	loss: BCE, ES: 30 epochs
Evaluation metrics	
Segmentation	Dice, IoU, Precision, AUCROC
Classification	AUCROC

P = population size, G = generations, C = contrast, B = brightness, M = mutation rate, Opt = optimizer, BS = batch size, ES = early stopping.

3.2 Illumination enhancement results

Figure 1 shows that IECET mainly improves brightness, but fails to enhance contrast or sharpness. In contrast, our GA-based method produces more balanced enhancements across all quality metrics. This is also confirmed in the 3D scatter plot (Figure 2).

*Corresponding Author.

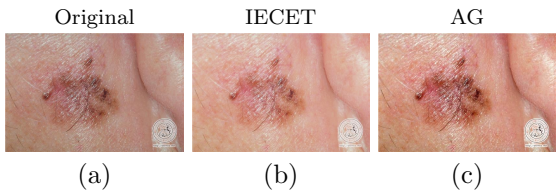

Figure 1. Visual example from the Waterloo dataset showing the effect of enhancement methods: (a) original, (b) IECET-enhanced, (c) GA-enhanced.

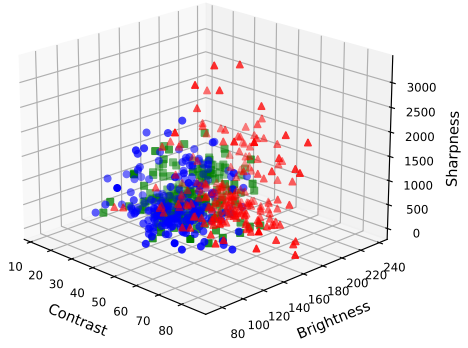

Figure 2. 3D scatter plot of image quality metrics (contrast, brightness, and sharpness) for three image sets: original (in blue), GA-enhanced (in red), and IECET-enhanced (in green).

3.3 Segmentation and classification performance

Table 2 summarizes segmentation metrics. GA-enhanced images combined with Attention U-Net yielded the best results, achieving a Dice score of 0.871 and AUCROC of 0.951. For melanoma detection, the best AUC-ROC (0.80) was achieved when using GA-enhanced and segmented images, as shown in Figure 3. This highlights the effectiveness of combining image enhancement and segmentation to improve classification performance.

Table 2. Segmentation metrics for U-Net variants using original, IECET-enhanced, and GA-enhanced images.

Image type	Model	DI	IoU	Precision	AUCROC
Original	U-Net	0.840±0.041	0.726±0.061	0.860±0.061	0.927±0.026
	Att-Net	0.868±0.035	0.769±0.054	0.896±0.043	0.944±0.022
	D-Net	0.866±0.032	0.765±0.050	0.881±0.040	0.937±0.019
IECET	U-Net	0.847±0.040	0.737±0.058	0.894±0.049	0.940±0.022
	Att-Net	0.851±0.040	0.745±0.065	0.899±0.039	0.943±0.021
	D-Net	0.846±0.036	0.735±0.064	0.875±0.052	0.932±0.025
GA	U-Net	0.859±0.035	0.755±0.053	0.881±0.021	0.935±0.011
	Att-Net	**0.871±0.049**	**0.775±0.074**	**0.913±0.020**	**0.951±0.010**
	D-Net	0.852±0.040	0.744±0.061	0.878±0.031	0.934±0.017

3.4 Interpretability analysis

To enhance transparency and interpretability, we used Grad-CAM to visualize CNN attention. As shown in Figure 4, original images (d) yield diffuse focus, often on irrelevant areas. GA-enhanced inputs (e) improve focus on lesions, and combining enhancement with segmentation (f) further sharpens attention, boosting relevance and interpretability.

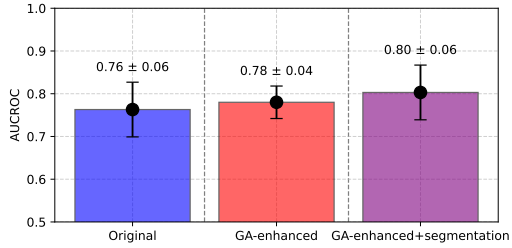

Figure 3. Mean±SD of AUCROC using ResNet-50 on original, GA-enhanced, and GA+segmentation images across 5 folds of the Waterloo dataset.

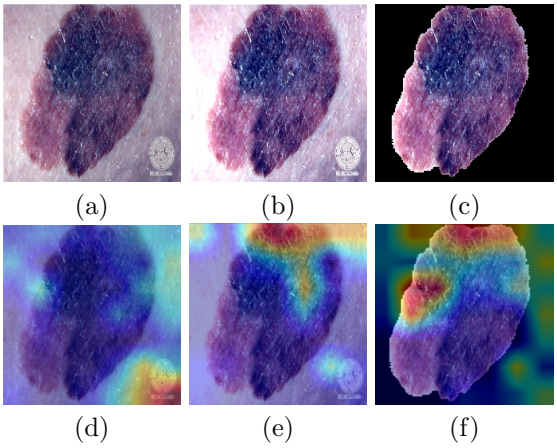

Figure 4. Example from the Waterloo dataset showing input types and their Grad-CAM heatmaps. Top row: (a) original, (b) GA-enhanced, (c) GA-enhanced + segmentation. Bottom row: corresponding Grad-CAM heatmaps for (d)–(f).

4 Conclusions

We propose a hybrid framework that combines unsupervised GA-based enhancement, U-Net segmentation, and ResNet-50 classification for macroscopic skin lesion analysis. Our method enhances image quality without reference data, tackling issues like low contrast and uneven lighting.

Experiments show improved segmentation across U-Net variants, with the best results from enhancement plus Attention U-Net. Melanoma detection also improves, achieving the highest AUCROC with GA-enhanced and segmented images. Grad-CAM analysis confirms better model focus on lesions, boosting interpretability and reducing irrelevant attention.

These results highlight the potential of our approach to support dermatological diagnosis using accessible imaging.

References

[1] Y. Sun et al. "Global trends in melanoma burden: a comprehensive analysis from the global burden of disease study, 1990-2021". In: *Journal of the American Academy of Dermatology* 92.1 (2025), pp. 100–107.

[2] K. D. Rojas et al. "Skin cancer: Primary, secondary, and tertiary prevention. Part II." In: *Journal of the American Academy of Dermatology* 87.2 (2022), pp. 271–288.

[3] V. Venugopal et al. "An EfficientNet-based modified sigmoid transform for enhancing dermatological macro-images of melanoma and nevi skin lesions". In: *Computer Methods and Programs in Biomedicine* 222 (2022), p. 106935.

[4] D. Liu. "Mathematical modeling analysis of genetic algorithms under schema theorem". In: *Journal of Computational Methods in Sciences and Engineering* 19.S1 (2019), pp. 131–137.

[5] N. Siddique et al. "U-net and its variants for medical image segmentation: A review of theory and applications". In: *IEEE Access* 9 (2021), pp. 82031–82057.

[6] K. He et al. "Deep residual learning for image recognition". In: *Proceedings of the IEEE Conference on Computer Vision and Pattern Recognition*. Las Vegas, Nevada, USA, June 2016, pp. 770–778.

[7] B. Zhou et al. "Learning deep features for discriminative localization". In: *Proceedings of the IEEE Conference on Computer Vision and Pattern Recognition (CVPR)*. Los Alamitos, CA, USA, June 2016, pp. 2921–2929.

[8] *Dermatology Information System*. http://www.dermis.net. 2012.

[9] *DermQuest*. http://www.dermquest.com. 2012.

[10] N. Razmjooy et al. "Computer-aided diagnosis of skin cancer: a review". In: *Current Medical Imaging* 16.7 (2020), pp. 781–793.

[11] C. H. Sudre et al. "Generalised dice overlap as a deep learning loss function for highly unbalanced segmentations". In: *Deep Learning in Medical Image Analysis and Multimodal Learning for Clinical Decision Support: Third International Workshop, DLMIA 2017, and 7th International Workshop, ML-CDS 2017, Held in Conjunction with MICCAI 2017, Proceedings 3*. Springer. Québec City, Québec, Canada, Sept. 2017, pp. 240–248.

[12] U. Ruby et al. "Binary cross entropy with deep learning technique for image classification". In: *International Journal of Advanced Trends in Computer Science and Engineering* 9.10 (2020).